Thin-film amorphous silicon germanium solar cells with p-and n-type hydrogenated silicon oxide layers

Si, Fai Tong; Isabella, Olindo; Zeman, Miro

DOI
10.1016/j.solmat.2017.01.001

Publication date
2017

Document Version
Final published version

Published in
Solar Energy Materials & Solar Cells

Solar Energy Materials & Solar Cells 163 (2017) 9–14

Contents lists available at ScienceDirect

Solar Energy Materials & Solar Cells

journal homepage: www.elsevier.com/locate/solmat

Thin-film amorphous silicon germanium solar cells with p- and n-type hydrogenated silicon oxide layers

Fai Tong Si*, Olindo Isabella, Miro Zeman

Photovoltaic Materials and Devices Laboratory, Delft University of Technology, Mekelweg 4, 2628 CD Delft, The Netherlands

ARTICLE INFO

Keywords:
Hydrogenated amorphous silicon germanium
Hydrogenated silicon oxide
Light management
Parasitic losses

ABSTRACT

Mixed-phase hydrogenated silicon oxide (SiO_x:H) is applied to thin-film hydrogenated amorphous silicon germanium (a-SiGe:H) solar cells serving as both p-doped and n-doped layers. The bandgap of p-SiO_x:H is adjusted to achieve a highly-transparent window layer while also providing a strong electric field. Bandgap grading of n-SiO_x:H is designed to obtain a smooth transition of the energy band edge from the intrinsic to n-doped layer, without the need of an amorphous buffer layer. With the optimized optical and electrical structure, a high conversion efficiency of 9.41% has been achieved. Having eliminated other doped materials without sacrificing performance, the sole use of SiO_x:H in the doped layers of a-SiGe:H cells opens up great flexibility in the design of high-efficiency multi-junction thin-film silicon-based solar cells.

1. Introduction

Hydrogenated amorphous silicon germanium (a-SiGe:H) is a meaningful building block in multi-junction thin-film silicon-based solar cells. Its electronic bandgap decreases as the Ge content increases in the matrix [1–3]. As an absorber material, a-SiGe:H offers an adjustable, intermediate bandgap between those given by the widely used hydrogenated amorphous silicon (a-Si:H, 1.7 eV) and hydrogenated nanocrystalline silicon (nc-Si:H, 1.1 eV). A combination of these absorbers can lead to better spectral utilization in triple- and quadruple-junction solar cells [4–7].

To form a p-i-n junction, p-type hydrogenated amorphous silicon carbide (a-SiC:H), a-Si:H, nc-Si:H, hydrogenated silicon oxide (SiO_x:H), and n-type a-Si:H, nc-Si:H, SiO_x:H have been used in the p- and n-layer, respectively, of a-SiGe:H solar cells. Among these materials, SiO_x:H is worth extra attention because of its multifunctionality and adaptability demonstrated in the application of thin-film silicon-based solar cells. SiO_x:H is a mixed-phase material comprising nanocrystalline silicon filaments embedded in an amorphous silicon oxide matrix [8–14]. The anisotropic growth of the material results in good transverse and poor lateral conductivity, thus improving the electrical performance of the solar cell. Optically, its relatively wide bandgap and low absorption coefficient suppress own parasitic absorption, while providing a high built-in voltage as a p-layer. The tunable refractive index offers a means to reduce the reflection at the window layer, or to enhance the intermediate reflection when used after an absorber layer [5,15–17]. Given that well-performing tunnel recombination junctions (TRJs) can be formed between p-type and n-type SiO_x:H [17], SiO_x:H opens a great versatility for the light management in multi-junction solar cells. Lastly, n-type SiO_x:H/Ag was also used to replace the typical ZnO:Al/Ag back reflector, as the low refractive index of SiO_x:H can limit the plasmonic absorption in Ag [18–20], just like in ZnO:Al/Ag stack. Fig. 1 shows the optical properties of the p- and n-type SiO_x:H, in comparison to other typical materials used in a-SiGe:H cells.

So far, the use of SiO_x:H in a-SiGe:H solar cells is not as popular as it is in a-Si:H or nc-Si:H cells. N-type SiO_x:H has been used as the n-layer of a-SiGe:H cells behind either intrinsic a-Si:H [6] or a-Si:H/nc-Si:H [21] buffer layer(s). On the p-side, Schüttauf et al. tested several p-layer configurations and reported a significant drop in V_{OC} when the p-layer was solely constituted of p-type SiO_x:H, compared to those which also include a a-SiC:H or a-Si:H layer between the oxide layer and the absorber [6]. Nevertheless, taking into account the adaptability of SiO_x:H materials and its successful applications in a-Si:H and nc-Si:H solar cells, it is natural to think of making a a-SiGe:H cell using only SiO_x:H for the doped layers, without compromising the performance. From the optical perspective, it can reduce the parasitic absorption caused by the other more absorptive supporting materials, and at the same time provide the most flexibility in light management for both single- and multi-junction devices. Electrically, the doped SiO_x:H materials can be tuned such that they give favorable band offset at the interfaces, or form efficient TRJs with minimized losses. In this paper, we explore the possibility of using both p- and n-type SiO_x:H in thin-film a-SiGe:H solar cells without extra buffer layers adjacent to the

* Corresponding author.
E-mail addresses: f.t.si@tudelft.nl (F.T. Si), o.isabella@tudelft.nl (O. Isabella), m.zeman@tudelft.nl (M. Zeman).

http://dx.doi.org/10.1016/j.solmat.2017.01.001
Received 8 December 2016; Accepted 2 January 2017
Available online 12 January 2017

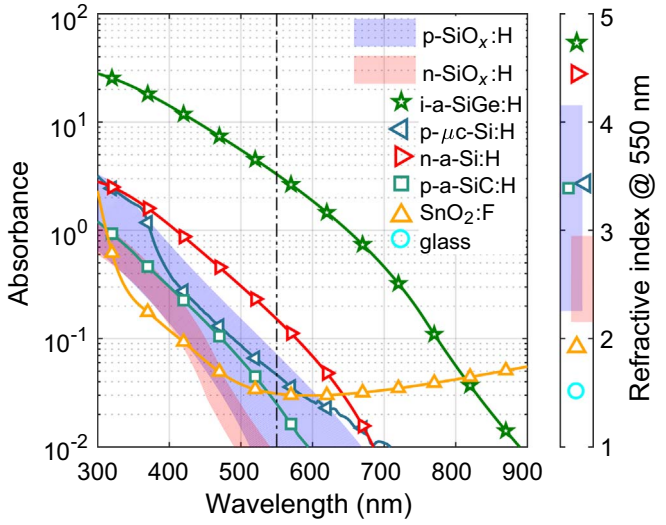

Fig. 1. Optical properties of typical materials used in a-SiGe:H solar cells: (Left) Absorbance $A = \alpha \cdot d$, where α is the absorption coefficient and d is the typical thickness of the material used in a device; (Right) Refractive index at wavelength λ=550 nm. The shaded areas in blue and red color represent the adjustable properties of p and n-type SiO_x:H, respectively. (For interpretation of the references to color in this figure legend, the reader is referred to the web version of this article.)

absorber layer. Additionally, we evaluate the performance of n-SiO_x:H/Ag back reflectors and optimize the light management of such device.

2. Experimental

The thin-film silicon alloy materials, including intrinsic a-SiGe:H, p- and n-type SiO_x:H and n-type a-Si:H, were deposited in a cluster tool using plasma-enhanced chemical vapor deposition (PECVD) at radio frequency (RF) of 13.56 MHz. The maximum substrate area and electrode area are 100 cm^2 and 144 cm^2 in square, respectively. Silane, germane and carbon dioxide were used as the source of silicon, germanium and oxygen, respectively. Diborane and phosphane (phosphine) were used as the doping gas for the p- and n-type materials, respectively. The deposition conditions of the PECVD materials are summarized in Table 1.

Thin-film a-SiGe:H solar cells were deposited on glass coated with nanotextured SnO_2:F (Asahi VU-type, Asahi Glass Co., Ltd. [22]) in superstrate p-i-n configuration. The typical device structure is glass/SnO_2:F/ZnO:Al/p-layer/i-a-SiGe:H/n-layer/Ag/Cr/Al. A thin layer of 20-nm-thick ZnO:Al was deposited using RF magnetron sputtering to protect the SnO_2:F against hydrogen plasma in the PECVD process [23]. The p-layer consists of a 4-nm-thick p-nc-Si:H on top of the front transparent conductive oxide (TCO) forming a good ohmic contact [14], and a 12-nm-thick p-SiO_x:H as the main p-type material for providing the electric field. The total thickness of the intrinsic a-SiGe:H is 200 nm. To mitigate the transportation barrier caused by the misalignment of energy bands between the intrinsic and doped materials [24–27], U-shape bandgap grading was applied by linearly reducing the GeH_4 flow in the a-SiGe:H deposition near the p-i and i-n interfaces. The thickness of the graded layers is 70 nm and 50 nm at the p- and n-side, respectively. It leaves the middle part of the intrinsic layer, which has the lowest bandgap, 80 nm in thickness. The n-layer is made of either n-a-Si:H, n-SiO_x:H, or a combination of the two. The Ag/Cr/Al metal stack with thicknesses of 300/30/800 nm serves as the back reflector as well as back electrode. It was deposited by thermal (Ag) or e-beam (Cr/Al) evaporation with a shadow mask so that the patterned metallic pad also defines the cell area. There are 30 cells on each sample and each cell has a squared area of 16 mm^2. Cell isolation was completed by etching away the materials outside the metal pads using anisotropic reactive ion etching (RIE). In occasions that ZnO:Al is used after the deposition of n-layer, the samples were dipped in diluted hydrochloric acid to remove the ZnO:Al prior to RIE.

The optical properties of the thin-film materials were characterized by spectroscopic ellipsometry (SE). The measurements were conducted at multiple incident angles using an M – 2000DI® Spectroscopic Ellipsometer (J.A. Woollam Co.), which is equipped with a dual-lamp light source covering the wavelength range of 193–1690 nm. To determine the optical bandgap of a-SiGe:H, the Tauc-Lorentz model [28,29] was fitted to the SE data measured from samples of single thin films deposited on glass substrates, and the result gave the optical bandgap E_{Tauc}. In addition, optical bandgap E_{04} was found as the energy with which a photon has an absorption coefficient of 1×10^4 cm^{-1} in the material.

The performance of the solar cells was examined by the illuminated current-voltage (*I-V*) measurement and external quantum efficiency (EQE) measurement. The *I-V* measurement was conducted at a controlled cell temperature of 25 °C, with a dual-lamp continuous solar simulator (WACOM WXS-90S-L2, class AAA). The two filtered lamps in the solar simulator were adjusted with two monocrystalline silicon reference cells manufactured by and traceable to the Fraunhofer Institute for Solar Energy Systems (ISE), to provide an incident irradiance of 1000 W m^{-2} with optimum spectral matching with AM1.5G solar spectrum. The EQE measurement was performed using an in-house system, in which the electrical signal is detected by a lock-in amplifier, and the chopped monochromatic light is provided by a xenon light source, a 3-grating monochromator and a chopper. A silicon photodiode, which was regularly calibrated by Fraunhofer ISE, was used to calibrate the light source in the EQE measurement. As for the external parameters of the solar cells, the open-circuit voltage (V_{OC}) and fill-factor (*FF*) are determined by the *I-V* measurement, while the short-circuit current density (J_{SC}) is calculated by weighting the measured EQE with the AM1.5G solar spectrum. The cell performance reported in this work is the average taken from the 12 better performing cells (40%) out of the 30 cells on each sample. While the EQE measurement was conducted on the best performing cell in each sample, the reported deviation in J_{SC} was obtained from the *I-V* measurement.

3. Results and discussion

3.1. Use of SiO_x:H in p-layer

In this section, p-SiO_x:H is applied in a-SiGe:H cells as the main p-layer, and the cell performance is examined. To compare the effect of different p-SiO_x:H, the device structure except the p-layer was kept the

Table 1
Deposition conditions of the PECVD materials used in this work. The constitution of gaseous precursors is shown by their flow rates in standard cubic centimeter per minute (sccm).

Material	*T* (°C)	*p* (mbar)	*P* (mW cm^{-2})	SiH_4	GeH_4	H_2	B_2H_6	PH_3	CO_2
p-nc-Si:H	180	2.2	243.1	0.8	–	190	0.004	–	–
p-SiO_x:H		2.2	90.3	0.8	–	190	0.004	–	0.8–2.2
i-a-SiGe:H		3.6	20.8	30.0	3.65	200	–	–	–
n-a-Si:H		0.6	27.8	40.0	–	10.8	–	0.22	–
n-SiO_x:H		1.5	69.4	1.0	–	101	–	0.024	0.5–2.6

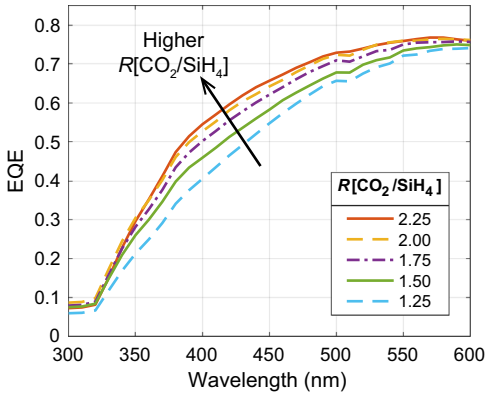

Fig. 2. EQE of a-SiGe:H cells with p-layers deposited at different concentration of CO_2. The spectra were measured at bias voltage V_{bias} = − 0.5 V, to feature the optical effect.

same as described in Section 2. No buffer layers were used between the p-i nor i-n interface. A series of solar cells were fabricated with different CO_2 flow rate during the deposition of p-layer. The different oxygen content in p-SiO_x:H results in different optical bandgap and electrical conductivity of the material [17].

The optical effect of the different p-SiO_x:H layers is first investigated. The p-layers were deposited with a flow rate ratio $R[CO_2/SiH_4]$ from 1.00 to 2.75. External quantum efficiency was measured at a bias voltage of −0.5 V to reduce the influence of inefficient carrier collection and to estimate the optical absorption in the absorber layer. The measured result is shown in Fig. 2. It is clear that in the short wavelengths between 300 nm and 600 nm, the greater the CO_2 flow during the p-layer deposition, the higher spectral response the solar cell exhibits. The difference in blue response mainly comes from the parasitic absorption in the p-layer. With more CO_2, the deposited p-SiO_x:H has a larger optical bandgap and lower absorption coefficient, so it allows more high-energy photons to be utilized in the intrinsic layer and contribute to the photocurrent. Beyond 600 nm, the EQE is very similar between the cells (not shown) because the p-layers barely absorb any photons in that region.

Electrically, the cells in Fig. 2 show similar performance. With a lowest $E_{Tauc}(E_{04})$ of 1.41 eV(1.62 eV) in the intrinsic layer, all cells have a *FF* in the range of 54–56%, as shown in Fig. 3. The V_{OC} shows a slight still monotonic increase with increased CO_2, from 654 mV to 660 mV. For a a-SiGe:H absorber with a wider bandgap, however, the p-SiO_x:H has a greater impact on the electrical performance of the solar cell. When the absorber has an $E_{Tauc}(E_{04})$ of 1.45 eV(1.67 eV) at its lowest point, both V_{OC} and *FF* show a monotonic increase with ratio $R[CO_2/SiH_4]$, in the range of 1.00–2.75. Overall, the p-SiO_x:H with a wider bandgap gives a better performance in the solar cell, provided that the p-layer still has sufficient transverse conductivity.

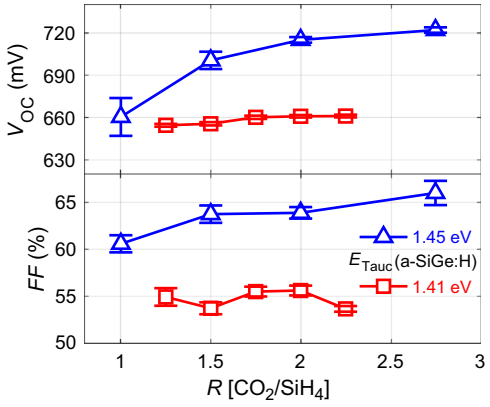

Fig. 3. External parameters V_{OC} and *FF* of a-SiGe:H cells with p-SiO_x:H made with different ratio of $R[CO_2/SiH_4]$.

3.2. Use of SiO_x:H in n-layer

In a-Si:H solar cells, both n-a-Si:H and n-SiO_x:H acting as the n-layer can lead to decent electrical performance of the cells. The use of n-SiO_x:H is more favorable when the optical losses and the behavior in forming TRJs [5,30] are considered. Based on such experience, several configurations of n-layer have been tested in this work to see how well they work for a-SiGe:H cells. The tested structures are summarized in Table 2. Configurations *a* and *e* comprise only a single layer of n-a-Si:H and n-SiO_x:H, respectively. The ratio $R[CO_2/SiH_4]$ for n-SiO_x:H was chosen to be 2.0 after some preliminary optimization. Configuration *b*, *c*, and *d* have the same n-SiO_x:H layer as *e*, but with an n-a-Si:H layer between the n-SiO_x:H and the intrinsic layers. Lastly, the deposition of configuration f started with a bandgap grading of n-SiO_x:H, in which the ratio $R[CO_2/SiH_4]$ was gradually changed from 1.0 to 2.0. The second half of the n-SiO_x:H deposition was then continued at $R[CO_2/SiH_4]$ of 2.0. The influence of different n-layer configurations was examined by the performance of the solar cells. A series of a-SiGe:H cells were fabricated using identical device structure except for the n-layer. p-SiO_x:H with $R[CO_2/SiH_4]$=2.0 was used as the p-layer and a-SiGe:H with a lowest E_{Tauc} of 1.45 eV was used as the i-layer.

The external parameters of the solar cells measured under AM1.5G spectrum are shown in Fig. 4. It is the most noticeable that configuration *a* provides significantly less photocurrent than all the others do. In this structure, the cell performance suffers from severe plasmonic absorption at the Ag back reflector because the adjacent material, which is n-a-Si:H, has a high refractive index [19]. From configuration *a*, with an additional n-SiO_x:H layer acting as an optical spacer, configuration *b* exhibits improved J_{SC} and slightly dropped *FF*. When comparing configurations *b*, *c* and *d*, the reduction of n-a-Si:H thickness mitigates the parasitic absorption, leading to the increase in J_{SC}. Furthermore, shrinking the defective n-a-Si:H layer also slightly improves V_{OC} and *FF*. n-SiO_x:H can act as n-type material to provide the necessary electric field, so the role of n-a-Si:H in these configurations is more about interface passivation and diminishing band offset. Without such buffer in between, configuration *e* gives worse V_{OC} and *FF* probably because of the band discontinuity between the absorber and the wide-gap n-SiO_x:H. To tackle this problem without using n-a-Si: H, configuration *f* aims at achieving a smooth transition from the intrinsic layer to narrow-gap n-SiO_x:H to wide-gap n-SiO_x:H by means of CO_2 grading during the deposition. As a result, all external parameters are improved from configuration *e* to *f*. Remarkably, this n-layer is solely constructed of n-SiO_x:H while its best sample tops the conversion efficiency among all compared configurations.

3.3. Optical spacer at back reflectors

It is demonstrated in Section 3.2 that because of its low refractive index, n-SiO_x:H can function as optical spacer at the back reflector to suppress the plasmonic absorption in Ag. Conventionally, ZnO:Al is

Table 2
Configurations of n-layer tested for a-SiGe:H cells.

#	Configuration
a	20 nm n-a-Si:H
b	20 nm n-a-Si:H/60 nm n-SiO_x:H
c	10 nm n-a-Si:H/60 nm n-SiO_x:H
d	5 nm n-a-Si:H/60 nm n-SiO_x:H
e	60 nm n-SiO_x:H
f	30 nm graded n-SiO_x:H/30 nm n-SiO_x:H

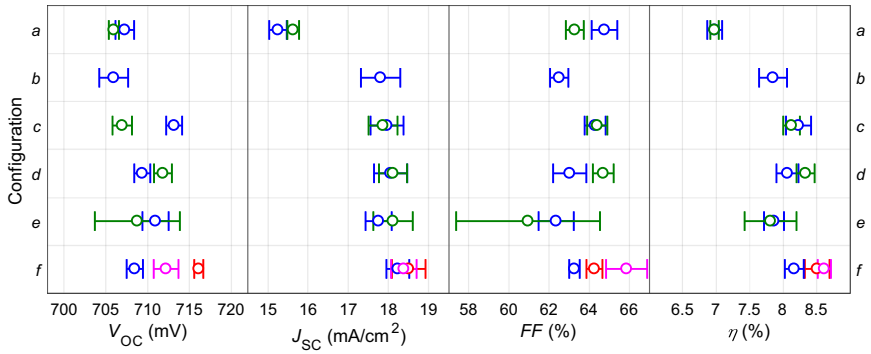

Fig. 4. External parameters of a-SiGe:H cells with different configurations of the n-layer. The multiple data sets (different colors) in a configuration represent samples having the same nominal structure but made in different deposition runs. The error bars are the standard deviation showing the inhomogeneity among the cells within a sample. (For interpretation of the references to color in this figure legend, the reader is referred to the web version of this article.)

used together with Ag back reflector for the same purpose [19]. On the other hand, the free carrier absorption in ZnO:Al [31] can potentially deteriorate the spectral response of the solar cell at long wavelengths.

In this section, we investigate the feasibility of fully replacing ZnO:Al with n-SiO_x:H in a-SiGe:H solar cells. A series of cells were fabricated with different configurations of optical spacer before the Ag back reflector. The basic structure includes p- and i-layers identical to the ones used in Section 3.2, as well as a 30-nm-thick n-SiO_x:H layer with bandgap grading. On top of it, wide-gap n-SiO_x:H and/or ZnO:Al with various thickness was deposited before completing the back reflector with Ag. The thicknesses of wide-gap n-SiO_x:H and ZnO:Al are 0/30 nm and 0/40/80/120 nm, respectively.

Fig. 5 shows the measured EQE of the a-SiGe:H cells with different spacer configurations. Without an additional layer of wide-gap n-SiO_x:H, it can be clearly seen in Fig. 5(a) that the spectral response at wavelengths longer than 700 nm is enhanced when the thickness of ZnO:Al is increased from 0 nm to 40 nm and further to 80 nm, showing the effect of ZnO:Al on reducing plasmonic absorption. When the thickness of ZnO:Al is further increased to 120 nm, the spectral response is not as good as the 80-nm-thick counterpart. We speculate that 80-nm-thick ZnO:Al is capable of quenching most of the plasmonic

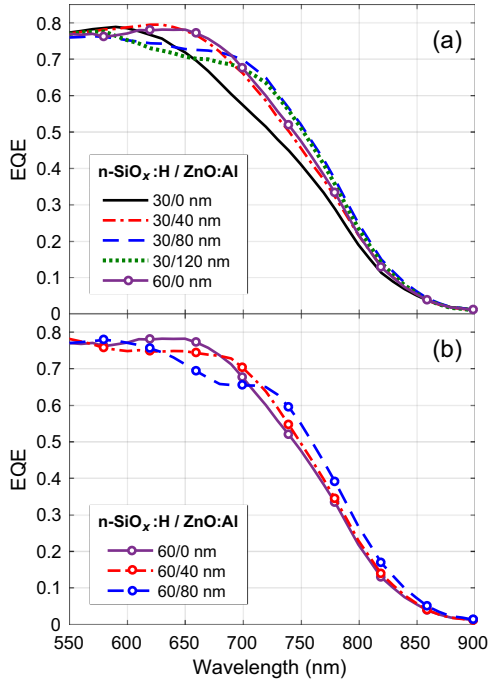

Fig. 5. EQE of a-SiGe:H cells with different thicknesses of n-SiO_x:H and ZnO:Al in front of the back reflector. The thickness of n-SiO_x:H is (a) 30 nm or (b) 60 nm in total. The result of the cell with 60-nm-thick n-SiO_x:H and no ZnO:Al is also plotted in (a) to show

absorption so the extra thickness of 40 nm only increases the parasitic absorption in ZnO:Al.

A direct comparison in Fig. 5(a) shows that the cell with 60/0 nm of n-SiO_x:H/ZnO:Al (i.e. no ZnO:Al) exhibits comparable spectral response to that of the cell with thinner n-SiO_x:H and 40-nm-thick ZnO:Al spacer. The addition of 30-nm-thick wide-gap n-SiO_x:H layer provides a similar effect as 40 nm of ZnO:Al. It confirms the capability of n-SiO_x:H material being an optical spacer to avoid parasitic losses. Fig. 5(b) shows the EQE spectra of cells with different thickness of ZnO:Al on top of the *extended* n-SiO_x:H layer. A similar improvement in the long wavelengths is observed when the thickness of ZnO:Al is increased, even with the thicker n-SiO_x:H layer. Two remarks should be noted for clarification: Firstly, all solar cells reported in Fig. 5 show similar V_{OC} and *FF*, so better spectral response can be translated to better cell performance. Secondly, the strong EQE variation between the samples in the wavelengths of 600–700 nm resembles the reflection spectrum of the respective cells (not shown). It is probably due to the interference effect, which is sensitive to the thickness of the films.

By extrapolation, one can expect comparable optical performance from replacing the thick ZnO:Al layer with a thick wide-gap n-SiO_x:H layer. Nonetheless, a thick wide-gap n-SiO_x:H layer can be too resistive to support efficient carrier transportation in the device. Therefore, a combination of n-SiO_x:H and ZnO:Al both with medium thickness should give the best overall performance.

3.4. Improvement by light scattering substrates

Light scattering is particularly important for a-SiGe:H solar cells. The intrinsic a-SiGe:H materials are rather defective compared to a-Si:H, so the absorber layer in a-SiGe:H cells has to be very thin to ensure adequate carrier collection efficiency of the device. Light scattering for enhancing the light absorption in the long wavelengths is therefore necessary for achieving high photocurrent within the thin absorber. In this section, the importance of light scattering for a-SiGe:H solar cells is highlighted by comparing cells fabricated on different light-scattering substrates.

The native roughness on APCVD SnO_2:F is too small to provide effective light scattering near the band edge of a-SiGe:H. On this respect, the surface of ZnO:B deposited by low-pressure CVD (LPCVD) typically features a greater roughness and larger (average) local surface inclination angle thus better light scattering capability among the longer wavelengths [32,33]. For comparison, solar cells were deposited on these two types of substrate, in specific, SnO_2:F (Asahi VU-type) and LPCVD ZnO:B with a thickness of 2.3 μm and smoothened by Ar plasma treatment for 4 min. The optimized device structure being used contains p-SiO_x:H with $R[CO_2/SiH_4]$=2.0, 60 nm of n-SiO_x:H with bandgap grading in its first half and $R[CO_2/SiH_4]$=2.0 in the second half, and 40 nm of ZnO:Al. In addition, the hydrogen dilution during a-SiGe:H deposition was slightly increased to improve the material

quality, while the ratio between SiH_4 and GeH_4 was maintained the same.

The performance of the optimized solar cells is shown in Fig. 6. On Asahi-VU substrates, the optimized device structure using doped SiO_x:H for both p- and n-layers delivers a conversion efficiency of 8.8%. For the cells on ZnO:B substrates, the V_{OC} and *FF* are fairly similar to that on Asahi-VU substrates. An obvious difference appears in the spectral response shown in Fig. 6(b). Except for wavelengths below 390 nm, at which ZnO:B is very absorptive, the cell made on ZnO:B shows a higher EQE over the whole spectrum of interest. It clearly demonstrates the difference in light scattering from different surface textures. The absorption enhancement leads to an improvement in J_{SC} from 18.4 mA/cm^2 on Asahi-VU to 19.5 mA/cm^2 on ZnO:B.

Finally, the optical loss from the reflection at the air/glass interface is tackled. An anti-reflection (AR) foil (produced by temicon GmbH) was applied onto the incident surface of the cell made on ZnO:B substrate. The influence of the AR treatment on the cell reflectance and EQE is shown in Fig. 6(b). At the wavelength of 550 nm, the reflectance is reduced from 5.8% to 3.9%, which corresponds to a reduction of 33%. The EQE in the visible spectrum is enhanced, consequently. In spite of the parasitic absorption induced by the AR foil in the short wavelengths, an increased J_{SC} of 19.8 mA/cm^2 is reached. In the end, as a result of the improved light management and optimized device structure, an efficiency of 9.41% is achieved.

4. Conclusions

Doped SiO_x:H was implemented in thin-film a-SiGe:H solar cells. In the window layer, the bandgap of p-SiO_x:H was adjusted to obtain a high V_{OC} and decent *FF*, while the transparency of the wide-gap p-layer also resulted in high spectral response in the short-wavelength region. The use of n-SiO_x:H instead of n-a-Si:H reduces the parasitic absorption in the n-layer and suppresses the plasmonic absorption in the neighboring metal layer. A combination of wide-gap n-SiO_x:H and TCO layers with appropriate thicknesses in front of a Ag back reflector provides the most favorable optical properties to enhancing the long-wavelength response of the solar cells. Bandgap grading of n-SiO_x:H was introduced and its application near the i-n interface mitigates the band offset between the wide-gap n-SiO_x:H and the absorber material. As a consequence, thin-film a-SiGe:H cells using only SiO_x:H doped layers have been realized without giving up the opto-electrical performance. Having optimized the cell structure, a conversion efficiency of 9.41% in a thin-film a-SiGe:H solar cell has been achieved on a ZnO:B-coated substrate with anti-reflection treatment. This study paves the way for designing high-efficiency thin-film silicon-based multi-junction solar cells with the use of a-SiGe:H absorber and multifunctional SiO_x:H layers.

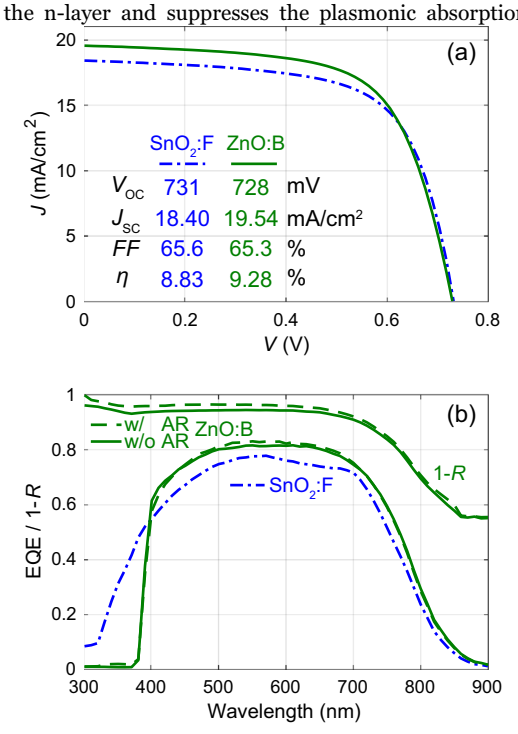

Fig. 6. (a) Current density-voltage (*J-V*) curves acquired under AM1.5G illumination, and (b) EQE measured at short-circuit condition, of the optimized a-SiGe:H cells fabricated on substrates with different light-scattering capability. Additionally, the EQE and 1-*R* spectra are given for the cells on ZnO:B substrate with (w/) and without (w/o) anti-reflection treatment.

Acknowledgements

The authors thank Dr. Hairen Tan for providing the ZnO:B substrates, which he prepared during a visiting research at the PV-Lab of IMT, EPFL in Neuchâtel, Switzerland.

This work was supported by the Foundation for Fundamental Research on Matter (FOM) (FOM-138-11SOL03), which is part of the Netherlands Organization for Scientific Research (NWO).

References

[1] B. von Roedern, D.K. Paul, J. Blake, R.W. Collins, G. Moddel, W. Paul, Optical absorption, photoconductivity, and photoluminescence of glow-discharge amorphous Si_1-xGe_x alloys, Phys. Rev. B 25 (12) (1982) 7678–7687. http://dx.doi.org/10.1103/PhysRevB.25.7678 (URL ⟨http://link.aps.org/doi/10.1103/PhysRevB.25.7678⟩).

[2] S. Guha, J. Payson, S. Agarwal, S. Ovshinsky, Fluorinated amorphous silicon-germanium alloys deposited from disilane-germane mixture, J. Non-Cryst. Solids 97–98 (1987) 1455–1458. http://dx.doi.org/10.1016/0022-3093(87)90349-8 (URL ⟨http://www.sciencedirect.com/science/article/pii/0022309387903498⟩).

[3] M. Stutzmann, R.A. Street, C.C. Tsai, J.B. Boyce, S.E. Ready, Structural, optical, and spin properties of hydrogenated amorphous silicon-germanium alloys, J. Appl. Phys. 66 (2) (1989) 569. http://dx.doi.org/10.1063/1.343574 (URL ⟨http://scitation.aip.org/content/aip/journal/jap/66/2/10.1063/1.343574⟩).

[4] J. Yang, A. Banerjee, S. Guha, Triple-junction amorphous silicon alloy solar cell with 14.6% initial and 13.0% stable conversion efficiencies, Appl. Phys. Lett. 70 (22) (1997) 2975. http://dx.doi.org/10.1063/1.118761 (URL ⟨http://scitation.aip.org/content/aip/journal/apl/70/22/10.1063/1.118761⟩).

[5] B. Yan, G. Yue, L. Sivec, J. Yang, S. Guha, C.-S. Jiang, Innovative dual function nc-SiOx:H layer leading to a >16% efficient multi-junction thin-film silicon solar cell, Appl. Phys. Lett. 99 (11) (2011) 113512. http://dx.doi.org/10.1063/1.3638068 (URL ⟨http://scitation.aip.org/content/aip/journal/apl/99/11/10.1063/1.3638068⟩).

[6] J.-W. Schüttauf, B. Niesen, L. Löfgren, M. Bonnet-Eymard, M. Stuckelberger, S. Hänni, M. Boccard, G. Bugnon, M. Despeisse, F.-J. Haug, F. Meillaud, C. Ballif, Amorphous silicon-germanium for triple and quadruple junction thin-film silicon based solar cells, Sol. Energy Mater. Sol. Cells 133 (2015) 163–169. http://dx.doi.org/10.1016/j.solmat.2014.11.006 (URL ⟨http://www.sciencedirect.com/science/article/pii/S0927024814005868⟩).

[7] D.J. You, S.H. Kim, H. Lee, J.-W. Chung, S.-T. Hwang, Y.H. Heo, S. Lee, H.-M. Lee, Recent progress of high efficiency Si thin-film solar cells in large area, Prog. Photovolt.: Res. Appl. 23 (8) (2015) 973–988. http://dx.doi.org/10.1002/pip.2510 (URL ⟨http://doi.wiley.com/10.1002/pip.2510⟩).

[8] P. Sichanugrist, T. Yoshida, Y. Ichikawa, H. Sakai, Amorphous silicon oxide with microcrystalline Si phase, J. Non-Cryst. Solids 164–166 (1993) 1081–1084. http://dx.doi.org/10.1016/0022-3093(93)91186-7 (URL ⟨http://www.sciencedirect.com/science/article/pii/0022309393911867⟩).

[9] P. Sichanugrist, T. Sasaki, A. Asano, Y. Ichikawa, H. Sakai, Amorphous silicon oxide and its application to metal/n-i-p/ITO type a-Si solar cells, Sol. Energy Mater. Sol. Cells 34 (1–4) (1994) 415–422. http://dx.doi.org/10.1016/0927-0248(94)90068-X (URL ⟨http://www.sciencedirect.com/science/article/pii/092702489490068X⟩).

[10] P. Cuony, M. Marending, D.T.L. Alexander, M. Boccard, G. Bugnon, M. Despeisse, C. Ballif, Mixed-phase p-type silicon oxide containing silicon nanocrystals and its role in thin-film silicon solar cells, Appl. Phys. Lett. 97 (21) (2010) 213502. http://dx.doi.org/10.1063/1.3517492 (URL ⟨http://scitation.aip.org/content/aip/journal/apl/97/21/10.1063/1.3517492⟩).

[11] R. Biron, C. Pahud, F.-J. Haug, J. Escarré, K. Söderström, C. Ballif, Window layer with p doped silicon oxide for high Voc thin-film silicon n-i-p solar cells, J. Appl. Phys. 110 (12) (2011) 124511. http://dx.doi.org/10.1063/1.3669389 (URL ⟨http://scitation.aip.org/content/aip/journal/jap/110/12/10.1063/1.3669389⟩).

[12] P. Cuony, D.T.L. Alexander, I. Perez-Wurfl, M. Despeisse, G. Bugnon, M. Boccard, T. Söderström, A. Hessler-Wyser, C. Hébert, C. Ballif, Silicon filaments in Silicon Oxide for next-generation photovoltaics, Adv. Mater. 24 (9) (2012) 1182–1186.

http://dx.doi.org/10.1002/adma.201104578 (URL ⟨http://doi.wiley.com/10.1002/adma.201104578⟩).
[13] L.V. Mercaldo, P. Delli Veneri, I. Usatii, E.M. Esposito, G. Nicotra, Properties of mixed phase n-doped silicon oxide layers and application in micromorph solar cells, Sol. Energy Mater. Sol. Cells 119 (2013) 67–72. http://dx.doi.org/10.1016/j.solmat.2013.05.030 (URL ⟨http://www.sciencedirect.com/science/article/pii/S0927024813002511⟩).
[14] H. Tan, P. Babal, M. Zeman, A.H. Smets, Wide bandgap p-type nanocrystalline silicon oxide as window layer for high performance thin-film silicon multi-junction solar cells, Sol. Energy Mater. Sol. Cells 132 (2015) 597–605. http://dx.doi.org/10.1016/j.solmat.2014.10.020 (URL ⟨http://www.sciencedirect.com/science/article/pii/S0927024814005510⟩).
[15] P. Buehlmann, J. Bailat, D. Dominé, A. Billet, F. Meillaud, A. Feltrin, C. Ballif, In situ silicon oxide based intermediate reflector for thin-film silicon micromorph solar cells, Appl. Phys. Lett. 91 (14) (2007) 143505. http://dx.doi.org/10.1063/1.2794423 (URL ⟨http://scitation.aip.org/content/aip/journal/apl/91/14/10.1063/1.2794423⟩).
[16] A. Lambertz, V. Smirnov, T. Merdzhanova, K. Ding, S. Haas, G. Jost, R. Schropp, F. Finger, U. Rau, Microcrystalline silicon-oxygen alloys for application in silicon solar cells and modules, Sol. Energy Mater. Sol. Cells 119 (2013) 134–143. http://dx.doi.org/10.1016/j.solmat.2013.05.053 (URL ⟨http://www.sciencedirect.com/science/article/pii/S0927024813002766⟩).
[17] H. Tan, E. Moulin, F.T. Si, J.-W. Schüttauf, M. Stuckelberger, O. Isabella, F.-J. Haug, C. Ballif, M. Zeman, A.H.M. Smets, Highly transparent modulated surface textured front electrodes for high-efficiency multijunction thin-film silicon solar cells, Prog. Photovolt.: Res. Appl. 23 (8) (2015) 949–963. http://dx.doi.org/10.1002/pip.2639 (URL ⟨http://doi.wiley.com/10.1002/pip.2639⟩).
[18] P. Delli Veneri, L.V. Mercaldo, I. Usatii, Silicon oxide based n-doped layer for improved performance of thin film silicon solar cells, Appl. Phys. Lett. 97 (2) (2010) 023512. http://dx.doi.org/10.1063/1.3463457 (URL ⟨http://scitation.aip.org/content/aip/journal/apl/97/2/10.1063/1.3463457⟩).
[19] V. Demontis, C. Sanna, J. Melskens, R. Santbergen, A.H.M. Smets, A. Damiano, M. Zeman, The role of oxide interlayers in back reflector configurations for amorphous silicon solar cells, J. Appl. Phys. 113 (6) (2013) 064508. http://dx.doi.org/10.1063/1.4790875 (URL ⟨http://link.aip.org/link/?JAP/113/064508/1⟩).
[20] H. Tan, E. Psomadaki, O. Isabella, M. Fischer, P. Babal, R. Vasudevan, M. Zeman, A.H.M. Smets, Micro-textures for efficient light trapping and improved electrical performance in thin-film nanocrystalline silicon solar cells, Appl. Phys. Lett. 103 (17) (2013) 173905. http://dx.doi.org/10.1063/1.4826639 (URL ⟨http://scitation.aip.org/content/aip/journal/apl/103/17/10.1063/1.4826639⟩).
[21] B. Liu, L. Bai, X. Zhang, C. Wei, Q. Huang, J. Sun, H. Ren, G. Hou, Y. Zhao, Fill factor improvement in PIN type hydrogenated amorphous silicon germanium thin film solar cells: omnipotent N type μc-SiOx:H layer, Sol. Energy Mater. Sol. Cells 140 (2015) 450–456. http://dx.doi.org/10.1016/j.solmat.2015.05.008 (URL ⟨http://www.sciencedirect.com/science/article/pii/S0927024815002135⟩).
[22] Asahi Glass Company, VU (TCO), TCO Coated glass for thin film application (a-Si/μc-Si). URL ⟨http://www.agc-solar.com/glass-products/coated-glass/tco/tco-vu.html⟩.
[23] M. Kubon, E. Boehmer, F. Siebke, B. Rech, C. Beneking, H. Wagner, Solution of the ZnO/p contact problem in a-Si:H solar cells, Sol. Energy Mater. Sol. Cells 41–42 (1996) 485–492. http://dx.doi.org/10.1016/0927-0248(95)00126-3 (URL ⟨http://www.sciencedirect.com/science/article/pii/0927024895001263⟩).
[24] S. Guha, J. Yang, A. Pawlikiewicz, T. Glatfelter, R. Ross, S.R. Ovshinsky, Band-gap profiling for improving the efficiency of amorphous silicon alloy solar cells, Appl. Phys. Lett. 54 (23) (1989) 2330. http://dx.doi.org/10.1063/1.101118 (URL ⟨http://scitation.aip.org/content/aip/journal/apl/54/23/10.1063/1.101118⟩).
[25] R. Jimenez Zambrano, F. Rubinelli, J. Rath, R. Schropp, Improvement in the spectral response at long wavelength of a-SiGe:H solar cells by exponential band gap design of the i-layer, J. Non-Cryst. Solids 299–302 (2002) 1131–1135. http://dx.doi.org/10.1016/S0022-3093(01)01080-8 (URL ⟨http://www.sciencedirect.com/science/article/pii/S0022309301010808⟩).
[26] B. Pieters, M. Zeman, R. van Swaaij, W. Metselaar, Optimization of a-SiGe:H solar cells with graded intrinsic layers using integrated optical and electrical modeling, Thin Solid Films 451–452 (2004) 294–297. http://dx.doi.org/10.1016/j.tsf.2003.11.029 (URL ⟨http://www.sciencedirect.com/science/article/pii/S0040609003015657⟩).
[27] J.-W. Chung, J.W. Park, Y.J. Lee, S.-W. Ahn, H.-M. Lee, O.O. Park, Graded layer modification for high efficiency Hydrogenated Amorphous Silicon-Germanium solar cells, Jpn. J. Appl. Phys. 51 (10S) (2012) 10NB16. http://dx.doi.org/10.1143/JJAP.51.10NB16 (URL ⟨http://iopscience.iop.org/article/10.1143/JJAP.51.10NB16⟩).
[28] G.E. Jellison, F.A. Modine, Parameterization of the optical functions of amorphous materials in the interband region, Appl. Phys. Lett. 69 (3) (1996) 371. http://dx.doi.org/10.1063/1.118064 (URL ⟨http://scitation.aip.org/content/aip/journal/apl/69/3/10.1063/1.118064⟩).
[29] G.E. Jellison, F.A. Modine, Erratum: parameterization of the optical functions of amorphous materials in the interband region, Appl. Phys. Lett. 69 (14) (1996) 2137. http://dx.doi.org/10.1063/1.118155 (URL ⟨http://scitation.aip.org/content/aip/journal/apl/69/14/10.1063/1.118155⟩).
[30] J. Fang, L. Bai, T. Li, G. Hou, B. Li, C. Wei, G. Wang, D. Zhang, Y. Zhao, X. Zhang, High-efficiency micromorph solar cell with light management in tunnel recombination junction, Sol. Energy Mater. Sol. Cells 155 (2016) 469–473. http://dx.doi.org/10.1016/j.solmat.2016.06.052 (URL ⟨http://www.sciencedirect.com/science/article/pii/S0927024816302252⟩).
[31] J. Sap, O. Isabella, K. Jäger, M. Zeman, Extraction of optical properties of flat and surface-textured transparent conductive oxide films in a broad wavelength range, Thin Solid Films 520 (3) (2011) 1096–1101. http://dx.doi.org/10.1016/j.tsf.2011.08.023 (URL ⟨http://www.sciencedirect.com/science/article/pii/S0040609011014842⟩, ⟨http://linkinghub.elsevier.com/retrieve/pii/S0040609011014842⟩).
[32] D. Dominé, The Role of Front Electrodes and Intermediate Reflectors in the Optoelectronic Properties of High-efficiency Micromorph Solar Cells (Ph.D. thesis), Université de Neuchâtel, 2009.
[33] K. Jäger, O. Isabella, R.A.C.M.M. van Swaaij, M. Zeman, Angular resolved scattering measurements of nano-textured substrates in a broad wavelength range, Meas. Sci. Technol. 22 (10) (2011) 105601. http://dx.doi.org/10.1088/0957-0233/22/10/105601 (URL ⟨http://stacks.iop.org/0957-0233/22/i=10/a=105601⟩).